UDC 621.3 https://doi.org/10.20998/2074-272X.2024.2.02

K. Abed, H.K.E. Zine

Intelligent fuzzy back-stepping observer design based induction motor robust nonlinear sensorless control

Introduction. *The control algorithm of Induction Motor (IM) is massively dependent on its parameters; so, any variation in these parameters (especially in rotor resistance) gives unavoidably error propagates. To avoid this problem, researches give more than solution, they have proposed Variable Structure Control (VSC), adaptive observers such as Model Reference Adaptive System, Extended Luenberger Observer (ELO) and the Extended Kalman Filter (EKF), these solutions reduce the estimated errors in flux and speed. As* ***novelty*** *in this paper, the model speed observer uses the estimated currents and voltages as state variables; we develop this one by an error feedback corrector. The Indirect Rotor Field Oriented Control (IRFOC) uses the correct observed value of speed; in our research, we improve the observer's labour by using back-stepping Sliding Mode (SM) control.* ***Purpose.*** *To generate the pulse-width modulation inverter pulses which reduce the error due of parameters variations in very fast way.* ***Methods.*** *We develop for reach this goal an exploration of two different linear observers used for a high performance VSC IM drive that is robust against speed and load torque variations. Firstly, we present a three levels inverter chosen to supply the IM; we present its modelling and method of control, ending by an experiment platform to show its output signal. A block diagram of IRFOC was presented; we analyse with mathematic equations the deferent stages of modelling, showed clearly the decoupling theory and the sensorless technique of control. The study described two kinds of observers, ELO and EKF, to estimate IM speed and torque. By the next of that, we optimize the step response using the fuzzy logic, which helps the system to generate the PI controller gains. Both of the two observers are forward by SM current controller, the convergence of SM-ELO and SM-EKF structures is guaranteed by minimizing the error between actual and observed currents to zero.* ***Results.*** *Several results are given to show the effectiveness of proposed schemes.* References 25, table 2, figures 9.

Key words: **induction motor, indirect rotor field oriented control, extended Kalman filter observer, extended Luenberger observer, fuzzy logic control, sliding mode control.**

Вступ. *Алгоритм керування асинхронним двигуном (АД) багато в чому залежить від його параметрів; тому будь-яка зміна цих параметрів (особливо опору ротора) неминуче призводить до поширення помилок. Щоб уникнути цієї проблеми, дослідники пропонують щось більше, ніж просто рішення: вони запропонували управління змінною структурою (VSC), адаптивні спостерігачі, такі як адаптивна система еталонної моделі, розширений спостерігач Люенбергера (ELO) та розширений фільтр Калмана (EKF); ці рішення зменшують передбачувані помилки за потоком та швидкістю.* ***Новизною*** *цієї статті є те, що спостерігач швидкості моделі використовує оцінені струми та напруги як змінні стани; ми розробляємо його за допомогою коректора зворотного зв'язку помилки. Непряме управління з полю ротора (IRFOC) використовує правильне значення швидкості; у нашому дослідженні ми покращуємо роботу спостерігача, використовуючи керування ковзним режимом (SM) зі зворотним кроком.* ***Мета***. *Генерувати імпульси інвертора широтно-імпульсної модуляції, які швидко зменшують помилку, викликану змінами параметрів.* ***Методи***. *Для досягнення цієї мети ми розробляємо дослідження двох різних лінійних спостерігачів, що використовуються для високопродуктивного приводу VSC АД, стійкого до змін швидкості та моменту навантаження. По-перше, ми представляємо трирівневий інвертор, вибраний для живлення АД; ми представляємо його моделювання та метод управління, закінчуючи експериментальною платформою, що демонструє його вихідний сигнал. Представлена блок-схема IRFOC; ми аналізуємо за допомогою математичних рівнянь різні етапи моделювання, наочно демонструючи теорію розв'язки та безсенсорний метод керування. У дослідженні описані два типи спостерігачів, ELO та EKF, для оцінки швидкості та крутного моменту АД. Далі ми оптимізуємо перехідну реакцію, використовуючи нечітку логіку, яка допомагає системі генерувати коефіцієнти посилення ПІ-регулятора. Обидва з двох спостерігачів передаються контролером струму SM, зближення структур SM-ELO та SM-EKF гарантується за рахунок зведення до нуля помилки між фактичним та спостережуваним струмами.* ***Результати***. *Наведено результати, що показують ефективність запропонованих схем.* Бібл. 25, табл. 2, рис. 9.

Ключові слова: **асинхронний двигун, непряме керування по полю ротора, розширений спостерігач фільтра Калмана, розширений спостерігач Люенбергера, керування нечіткою логікою, керування ковзним режимом.**

Introduction. Recently, in the literature researches develop Induction Motor (IM) control in modern methods, taking in consideration IM parameters variations as inputs and signal behaviors as wishes outputs, the implantation of modern observers in control schemes is more than necessary.

In several structures and families, observers take places in linear and non-linear configurations systems as important solution can deals with motors states variations in good manner; for example, in the case when IM parameters was changed, we can see in [1-7] that the researches use adaptive observer as solution to get a speed convergence, in [8-11] researches deal with this problem by using back-stepping control, which gives better results.

We can see also in [12-24] the using of fuzzy logic technique to observe the controller parameters. In [22] the writer gives a model of Sliding Mode (SM) observer powered by fuzzy logic technique in goal of minimizing the error surface. In [22, 24], they use fuzzy logic to esteem the PI or PID parameters (K_p and K_i) which vary with the IM parameters variation during system operation.

Purpose. In our work, we take a new reasoning method to preserve the system divergence when changing motor parameters (rotor resistance in our case). We propose the using of a Variable Structure Control (VSC) methodology in order to improve the system robustness, the application runs by the implementation of SM in two observers structures combining by Extended Luenberger Observer (ELO) and Extended Kalman Filter (EKF) is shown in [12-17] the system is vector-controlled by indirect rotor field control scheme.

Not only the control of parameters variations is reached in our proposed method; but the robustness is also ameliorated by using SM, which we can observe in

lateral conditions of speed and torque variations during system operation.

In addition, in our paper, we made a comparison between SM control and fuzzy logic technique, this comparison allowed us to select our prefer method which plays a role in the improvement of the IM nonlinear sensorless control.

The simulation results, in the end of work, are given to show the effectiveness of proposed control approach. Those results are obtained from a drive control algorithms in the laboratory, with the help of MATLAB tool.

Three levels voltage inverter. We can create Three Levels Inverter (3LI) voltages in complete bridges by collecting three half-bridges using capacitive divider structure (Fig. 1).

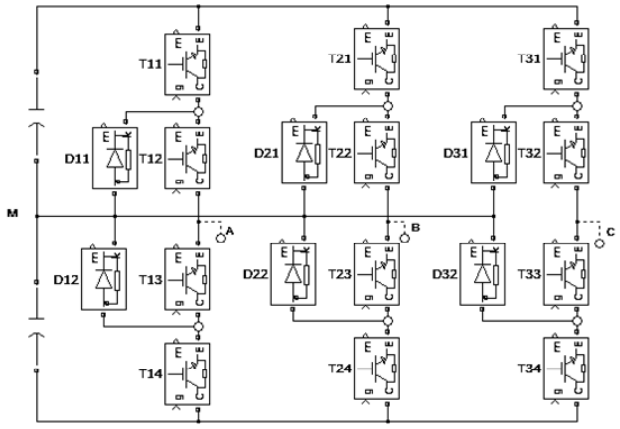

Fig. 1. Three Levels inverter Neutral Point Clamped (3LI-NPC)

1. Inverter's command strategy. The output voltages of 3LI are given in:

$$\begin{bmatrix} V_A \\ V_B \\ V_c \end{bmatrix} = \frac{1}{3}\begin{bmatrix} 2 & -1 & -1 \\ -1 & 2 & -1 \\ -1 & -1 & 2 \end{bmatrix} \cdot \left\{ \begin{bmatrix} B_{11}^b \\ B_{21}^b \\ B_{31}^b \end{bmatrix} \cdot U_{c1} - \begin{bmatrix} B_{10}^b \\ B_{20}^b \\ B_{30}^b \end{bmatrix} \cdot U_{c2} \right\}, \quad (1)$$

where B_{Ki} is the transistor's base command T_{Ki}.

Researchers have controlled the 3LI with deferent pulse-width modulation (PWM) strategies; in the next (Fig. 2 and Table 1) we present simulation and experimentation comparison between three strategies methods, we found that saw tooth-sinusoidal command is the better one to use; we use it, in this research, with two identical carriers. The experimental results in [18] were raised by using the acquisition card AT-MIO-16X through a current and voltage sensor card.

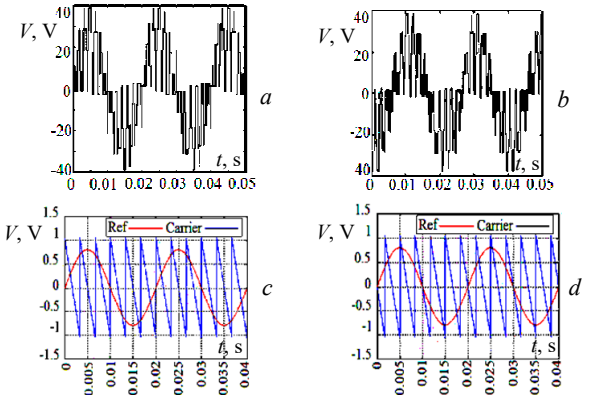

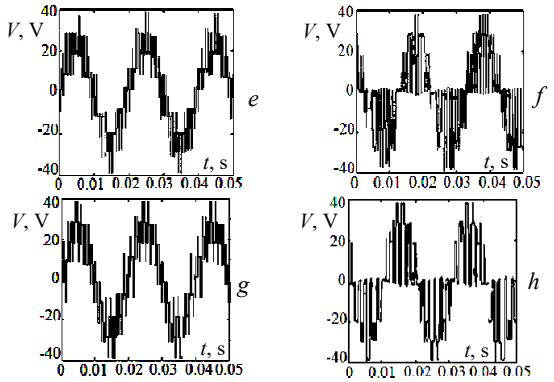

Fig. 2. Output voltage V_a as a function of time:
- triangular-sinusoidal command with one carrier simulation result in (*a*) and experimentation result in (*b*);
- principle of saw tooth-sinusoidal command with two carriers: reference voltage and saw tooth carrier 1 in (*c*) and reference voltage and saw tooth carrier 2 in (*d*);
- saw tooth-sinusoidal command with two carriers simulation result in (*e*) and experimentation result in (*f*);
- vector modulation strategy simulation result in (*g*) and experimentation result in (*h*)

Table 1
Comparison between harmonics of the various command types

Command strategy	THD max	THD min
Triangular-sinusoidal with one carrier	0.671	0.669
Saw-tooth-sinusoidal with two carriers	0.421	0.420
Vector modulation	0.498	0.497

2. Power stage. The IGBT transistor characteristics are: IRFBC40, 3 to 8 kHz, V_{CE} = 600 V, I_C = 49 A, V_{CE} (sat) ≤ 2 V, E_{TS} ≤ 9 mJ.

The commutation diode characteristics: BYT30PI 1000, V_{RRM} = 1 kV, I_F = 30 A, t_{rr} = 55 ns, V_S = 1.47 V.

Command stage:

- PIA card (Parallel Interface Adapter);
- a galvanic insulation card for the PC and card PIA protection;
- an interface card.

Sample of experimental installation is shown in Fig. 3.

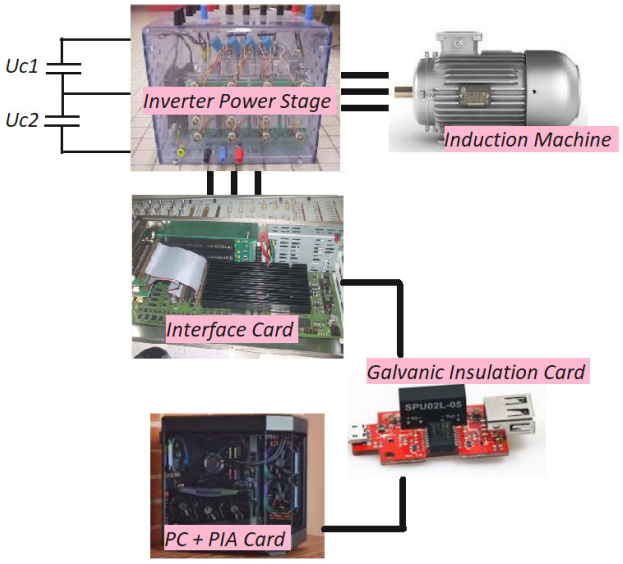

Fig. 3. Experimental installation constituents

Field oriented control structure. This plan uses a more robust strategy (Fig. 4), which exclude all kind of sensors in its algorithm.

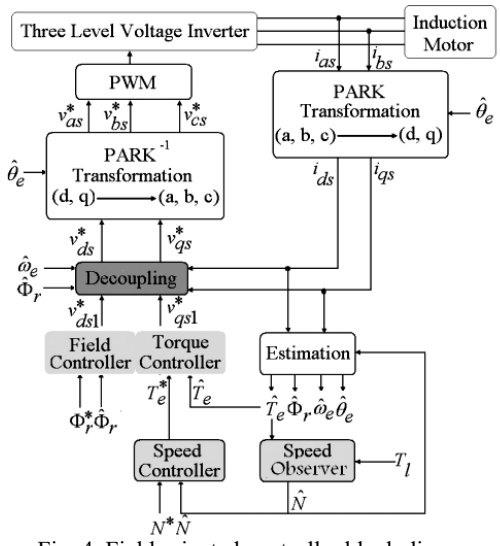

Fig. 4. Field oriented controller block diagram

The Indirect Rotor Field Oriented Control (IRFOC) proposes:

$$\begin{bmatrix} \frac{\mathrm{d}i_{ds}}{\mathrm{d}t} \\ \frac{\mathrm{d}i_{qs}}{\mathrm{d}t} \\ \frac{\mathrm{d}\phi_{dr}}{\mathrm{d}t} \\ \frac{\mathrm{d}\phi_{qr}}{\mathrm{d}t} \end{bmatrix} = \begin{bmatrix} -\gamma & \omega_e & \frac{k}{\tau_r} & p\cdot N\cdot k \\ -\omega_e & -\gamma & -p\cdot N\cdot k & \frac{k}{\tau_r} \\ \frac{L_m}{\tau_r} & 0 & -\frac{1}{\tau_r} & \omega_e - p\cdot N \\ 0 & \frac{L_m}{\tau_r} & -(\omega_e - p\cdot N) & -\frac{1}{\tau_r} \end{bmatrix} \begin{bmatrix} i_{ds} \\ i_{qs} \\ \phi_{dr} \\ \phi_{qr} \end{bmatrix} + \begin{bmatrix} \frac{1}{\sigma L_s} & 0 \\ 0 & \frac{1}{\sigma L_s} \\ 0 & 0 \\ 0 & 0 \end{bmatrix} \begin{bmatrix} v_{ds} \\ v_{qs} \end{bmatrix}, \quad (2)$$

where i_{ds}, i_{qs} are the *d*-*q* axis stator currents; v_{ds}, v_{qs} are the *d*-*q* axis stator applied voltages; ϕ_{dr}, ϕ_{qr} are the *d*-*q* rotor flux linkages; τ_r is the rotor time constant, $\tau_r = L_r/R_r$; ω_e is the synchronous angular speed; $k = M/\sigma L_s L_r$; γ, k are the simplifying constants; $\sigma = 1 - M^2/L_s L_r$; N is the estimated speed; L_s, L_r are the stator and rotor inductances; L_m is the mutual inductance; R_s, R_r are the stator and rotor winding resistances; M is the mutual magnetizing inductance; σ is the leakage coefficient; p is the number of pole pairs.

The decoupling between *d* and *q* axes can be realized by: $\Phi_{qr} = 0$; $\mathrm{d}\Phi_{qr}/\mathrm{d}t = 0$, and $\Phi_{dr} = \Phi_r$, where Φ_r is the rated flux. So:

$$\begin{cases} v_{ds} = \sigma L_s \dfrac{di_{ds}}{dt} + \left(R_s + R_r \dfrac{M^2}{L_r^2} \right) i_{ds} - \omega_e \sigma L_s i_{qs} - \dfrac{M}{L_r^2} R_r \Phi_r; \\ v_{qs} = \sigma L_s \dfrac{di_{qs}}{dt} + \omega_e \sigma L_s i_{qs} + \left(R_s + R_r \dfrac{M^2}{L_r^2} \right) i_{ds} - \dfrac{M}{L_r^2} pN\Phi_r; \\ \tau_r \dfrac{d\Phi_r}{dt} + \Phi_r = M i_{ds}; \\ \omega_e = pN + \dfrac{M}{\tau_r} \dfrac{i_{qs}}{\Phi_r}. \end{cases} \quad (3)$$

The mechanical equations, electromagnetic torque and motor speed are related by:

$$J\frac{\mathrm{d}N}{\mathrm{d}t} + fN = T_e - T_l, \quad (4)$$

where T_e, T_l are the electromagnetic and load torques; f is the friction coefficient; J is the total inertia.

The expression of electromagnetic torque is:

$$T_e = p\frac{M}{L_r}\Phi_r i_{qs}. \quad (5)$$

The decoupled system is given by:

$$\begin{cases} v_{ds}^* = v_{ds1} - e_{ds}; \\ v_{qs}^* = v_{qs1} - e_{qs}, \end{cases} \quad (6)$$

where

$$\begin{cases} e_{ds} = \hat{\omega}_e \sigma L_s i_{qs} + \dfrac{M}{L_r^2} R_r \Phi_r; \\ e_{qs} = -\hat{\omega}_e \sigma L_s i_{ds} - \dfrac{M}{L_r} \hat{\omega}_e \Phi_r + \dfrac{M^2}{L_r \tau_r} i_{qs}, \end{cases} \quad (7)$$

where «^» is the estimated value; «*» is the reference value.

Sensorless speed control design. The estimation of synchronous angular speed is calculated by using the row 4 in (3):

$$\omega_e = pN + \frac{M}{\tau_r}\frac{i_{qs}}{\hat{\Phi}_r + \varepsilon}, \quad (8)$$

where $\hat{\Phi}_r$ is the estimate flux; $\varepsilon = 0.01$ is the constant to avoid the mathematical divergence when $\hat{\Phi}_r \approx 0$.

From the row 3 of (3) we estimate:

$$\hat{\Phi}_r = \frac{M}{1 + \tau_r p} i_{ds}.$$

Speed control. From the synchronous angular speed, we obtained $\theta_e = \int \omega_e \mathrm{d}t$. To estimate the speed, we establish following function:

$$N = \frac{1}{Jp + f}(T_e - T_l). \quad (9)$$

Closed loop Luenberger observer implantation. Several researches use ELO in sensorless control of IM [14, 16, 17], the goal is to remove all mechanical sensors. From (4) and (5) we have:

$$\frac{\mathrm{d}N}{\mathrm{d}t} = -\frac{f}{J}N + \frac{pM\Phi_r}{JL_r} i_{qs} - \frac{1}{J}T_l. \quad (10)$$

The 2nd order ELO is given by: $\begin{cases} \dot{\hat{X}} = A\hat{X} + BU + L(Y - \hat{Y}); \\ \hat{Y} = C\hat{X}, \end{cases}$

where $\hat{X} = \begin{bmatrix} N_{obs} \\ T_{l-obs} \end{bmatrix}$, $L = \begin{bmatrix} l_1 \\ l_2 \end{bmatrix}$, and we have finally:

$$\begin{bmatrix} \frac{\mathrm{d}N_{obs}}{\mathrm{d}t} \\ \frac{\mathrm{d}T_{l-obs}}{\mathrm{d}t} \end{bmatrix} = \begin{bmatrix} -\frac{f}{J} - l & \frac{-1}{J} \\ -l_2 & 0 \end{bmatrix} \begin{bmatrix} N_{obs} \\ T_{l-obs} \end{bmatrix} + \begin{bmatrix} \frac{pM\Phi_r}{JL_r} \\ 0 \end{bmatrix} (i_{qs}) + \begin{bmatrix} l_1 \\ l_2 \end{bmatrix} \cdot N, \quad (11)$$

where N_{obs} is the observed speed; T_{l_obs} is the observed load torque. We put $l_1 = 250$, $l_2 = -600$ to fix the observer dynamics.

Control with extended Kalman filter observer. EKF offers the estimation of the systems states [12, 13]. The forward approximation is used to discretize (2):

$$\begin{cases} x(k+1) = f(x(k), k) + g(u(k), k); \\ y(k) = h(x(k), k), \end{cases} \quad (12)$$

where

$$f(x(k), k) + g(u(k), k) = A_d x(k) + B_d u(k);$$
$$A_d = I + A_c T_s;\ B_d = B_c T_s;$$

$$A_c=\begin{bmatrix} -\gamma & \omega_e & k/\tau_r & pNk \\ -\omega_e & -\gamma & -pNk & k/\tau_r \\ L_m/\tau_r & 0 & -1/\tau_r & \omega_e-pN \\ 0 & L_m/\tau_r & -(\omega_e-pN) & -1/\tau_r \end{bmatrix}; B_c=\begin{bmatrix} \frac{1}{\sigma L_S} & 0 \\ 0 & \frac{1}{\sigma L_S} \\ 0 & 0 \\ 0 & 0 \end{bmatrix}, \quad (13)$$

where $T_s = (t_k - t_{k-1})$ is the sampling time.

The stochastic model of the disturbances is established by adding noise vectors as below:

$$\begin{cases} \hat{x}(k+1) = f(\hat{x}(k),k) + g(u(k),k) + w(k); \\ y(k) = h(\hat{x}(k),k) + v(k), \end{cases} \quad (14)$$

where $u(k)$, $y(k)$ are the input and output signals; $w(k)$ is the process noise; $v(k)$ is the measurement one; $x(k)$ is the state vector, which can be observed by the EKF as:

$$\hat{x}(k+1) = f(\hat{x}(k),k) + g(u(k),k) + K_e\left[y(k) - h(\hat{x}(k),k)\right]. \quad (15)$$

By using Riccati difference equation, we can establish the Kalman gain K_e and we can simplify it as:

$$K_e = \begin{bmatrix} 0 & 0 & 0 \\ k_{e1} & k_{e2} & k_{e3} \end{bmatrix}^T \begin{bmatrix} \cos\hat{\theta}_e & \sin\hat{\theta}_e \\ -\sin\hat{\theta}_e & \cos\hat{\theta}_e \end{bmatrix}, \quad (16)$$

where k_{e1}, k_{e2}, k_{e3} are the adjustable parameters, and:

$$h(x(k)) = \left[\cos\hat{\theta}_e(k) \quad \sin\hat{\theta}_e(k)\right]^T.$$

The output variables of the EKF may be chosen as:

$$\left[y_1(k), y_2(k)\right] = \left[\Phi_{\beta s}, \Phi_{\alpha s}\right], \quad (17)$$

where $\Phi_{\alpha s}$, $\Phi_{\beta s}$ are the α-β stator flux linkages.

When $x = \left[\hat{\theta}_e \quad \hat{w}_e \quad w'\right]^T$ are the state variables with w' as the double integration of noise.

When we put $u(k) = 0$, the model (14) can be written as:

$$\begin{cases} \hat{x}(k+1) = F(\hat{x}(k)) + w(k); \\ y(k) = h(\hat{x}(k)) + v(k), \end{cases} \quad (18)$$

where

$$F = \begin{bmatrix} 1 & T_s & 0 \\ 0 & 1 & 1 \\ 0 & 0 & 1 \end{bmatrix}.$$

So, $\hat{w}_e$ and $\hat{\theta}_e$ can be observed by:

$$\hat{w}_e(p) = \frac{\mathrm{d}\hat{\theta}_e(p)}{\mathrm{d}t} = \frac{\hat{\theta}(k+1) - \hat{\theta}(k)}{T_s} = \hat{w}_e(k) + k_1\varepsilon(k); \quad (19)$$

$$\hat{w}_e(k+1) - \hat{w}_e(k) = w'(k) + k_2\varepsilon(k); \quad (20)$$

$$w'(k+1) - w'(k) = k_3\varepsilon(k); \quad (21)$$

$$\varepsilon(k) = y_2(k)\cos\hat{\theta}_e(k) - y_1(k)\sin\hat{\theta}_e(k). \quad (22)$$

The block diagram of the EKF used is shown in Fig. 5.

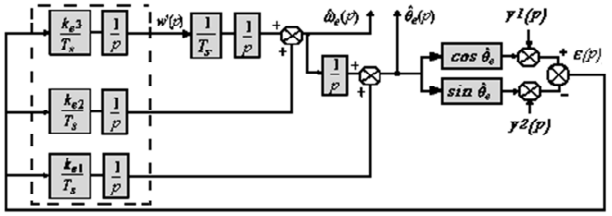

Fig. 5. Simplified EKF observer block diagram

SM current and flux observer design. The application of SM control to IMs has been widespread in [8-11, 22]; we implant it to estimate the speed and rotor time constant, our method guarantees the convergence of the current during control time and produces, as well, fluxes along the *d* and *q* axes. From (2) we can write:

$$\begin{bmatrix} \frac{\partial\hat{i}_{ds}}{\partial t} \\ \frac{\partial\hat{i}_{qs}}{\partial t} \end{bmatrix} = -\gamma\begin{bmatrix} \hat{i}_{ds} \\ \hat{i}_{qs} \end{bmatrix} + k\begin{bmatrix} \Psi_{dr} \\ \Psi_{qr} \end{bmatrix} + \frac{1}{\sigma L_S}\begin{bmatrix} v_{ds} \\ v_{qs} \end{bmatrix}; \quad (23)$$

$$\begin{bmatrix} \frac{\partial\hat{\Phi}_{dr}}{\partial t} \\ \frac{\partial\hat{\Phi}_{qr}}{\partial t} \end{bmatrix} = \frac{M}{\tau_r}\begin{bmatrix} i_{ds} \\ i_{qs} \end{bmatrix} - \begin{bmatrix} \Psi_{dr} \\ \Psi_{qr} \end{bmatrix}, \quad (24)$$

where

$$\Psi_{dr} = -u_{ds}\mathrm{sign}(s_{ds}); \qquad \Psi_{qr} = -u_{qs}sign(s_{qs});$$

$$u_{ds} = \left|-\gamma\bar{i}_{ds} - k\left(\frac{\phi_{dr}}{T_r} + pN\phi_{qr}\right)\right|;$$

$$u_{qs} = \left|-\gamma\bar{i}_{qs} - k\left(\frac{\phi_{qr}}{T_r} + pN\phi_{dr}\right)\right|, \quad (25)$$

where $\bar{i}_{ds} = \hat{i}_{ds} - i_{ds}, \bar{i}_{qs} = \hat{i}_{qs} - i_{qs}$;

$$\begin{bmatrix} \Psi_{dr} \\ \Psi_{qr} \end{bmatrix} = \begin{bmatrix} \frac{1}{\hat{\tau}_r} & p\hat{N}k \\ -p\hat{N}k & \frac{1}{\hat{\tau}_r} \end{bmatrix}\begin{bmatrix} \hat{\Phi}_{dr} \\ \hat{\Phi}_{qr} \end{bmatrix}, \quad (26)$$

and $s_{ds} = \hat{i}_{ds} - i_{ds}$; $s_{qs} = \hat{i}_{qs} - i_{qs}$.

So, speed and real value of the rotor time constant can be calculated by:

$$\begin{bmatrix} \frac{1}{\hat{\tau}_r} \\ p\hat{N}k \end{bmatrix} = \frac{1}{\left|\hat{\Phi}_r\right|}\begin{bmatrix} -\hat{\Phi}_{dr} & -\hat{\Phi}_{qr} \\ -\hat{\Phi}_{qr} & \hat{\Phi}_{dr} \end{bmatrix}\begin{bmatrix} \Psi_{dr} \\ \Psi_{qr} \end{bmatrix}, \quad (27)$$

where $\left|\hat{\Phi}_r\right| = (-\hat{\Phi}_{dr}^2 - \hat{\Phi}_{qr}^2)$.

Fuzzy-PI controller architecture. It has been developed recently in [19-24], we use fuzzy logic algorithm, as a smart attitude, to reconstruct the rotor resistance and load time constant, after their variations. The fuzzy part in the controller adjusts the PI gains, which planned to enhance the step feedback; the improvement of PI observers has been developed in other way by [25].

The speed error and its rate of change are the controller inputs, the K_i and K_p are its outputs, $e(k) = \overset{*}{N} - \hat{N}$ and $\Delta e(k) = e(k) - e(k-1)$

The program uses such linguistic tags: NL (Negative Large), NM (Negative Medium), NS (Negative Short), ZE (Zero), PS (Positive Short), PM (Positive Medium), PL (Positive Large). Every fuzzy tag has a related membership function. «*Set if then*» is the logic sentence, which represents the fuzzy control rules, these rules are formulated as follows: **If** $e(k)$ is NL **and** $\Delta e(k)$ is N **then** $T_e^*(k)$ is ZE. Results for speed control are shown in Table 2 with E is the error, CE is the convergence of error.

Table 2

Control rule base

$\downarrow CE / E\rightarrow$	NL	NM	NS	ZE	PS	PM	PL
N	ZE	S	M	L	M	S	ZE
ZE	ZE	S	M	L	M	S	ZE
P	ZE	M	L	L	L	M	ZE

To produce the inference mechanism, we use Mamdani Max-Min method (Fig. 6). We apply the center of gravity process to crisp the output value in the defuzzification stage:

$$\Delta\mu_0 = \sum_{j=0}^{n} C^0(\Delta\mu_j)\Delta\mu_j \Big/ \sum_{j=0}^{n} C^0(\Delta\mu_j). \quad (28)$$

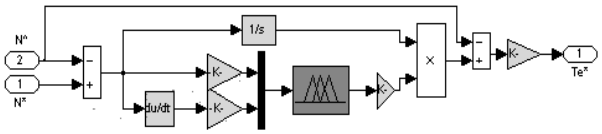

Fig. 6. Synoptic model of fuzzy controller for IM

Results and analysis. We consider the IM as continuous model. The IGBT based inverter is a 3LI-NPC, controlled by an 18 kHz PWM. The robustness of sensorless speed control is verified, in the first, we apply varied load torque values as: +10 N·m in 1 s, –10 N·m in 2.5 s, +10 N·m in 6 s, –10 N·m in 7 s, 0 N·m in 8 s with flux 0.8 Wb. The speed is fixed at 150 then –150 rad/s into 3.5 s.

In Fig. 7,*a* we show, obviously, that the dynamic performances of the speed are very good.

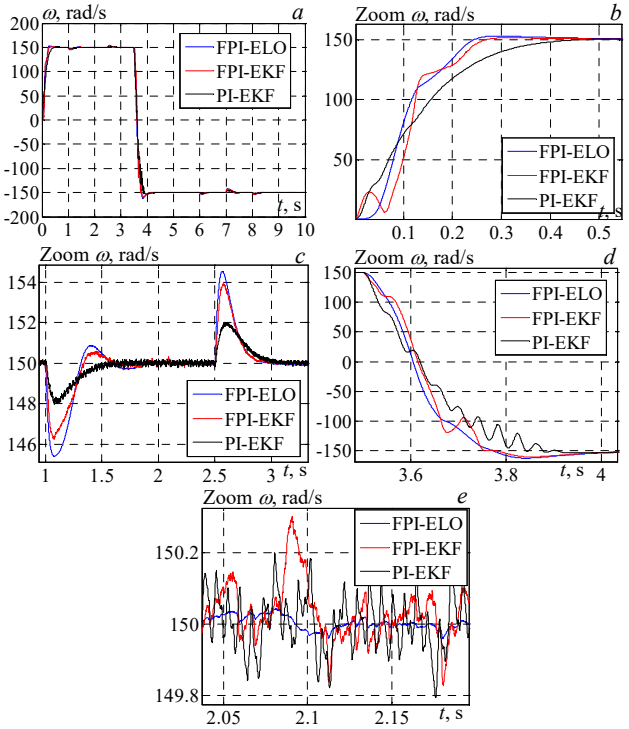

Fig. 7. Simulation results of the improved EKF and ELO observer by FPI controller: IM speed in (*a*); zoom in speed gives a comparison between the observer's time responses in (*b*); zoom in speed during control shows the speed overshoots in (*c*); speed delay time during the change of the speed reference in (*d*); harmonics observed during control in (*e*)

Presented in Fig. 7,*b* the Fuzzy Proportional-Integral FPI-ELO gives the better time response; it is more reliable and less-noise than the FPI-EKF (Fig. 7,*d* and Fig. 7,*e*). But it makes a slightly overshoot as shown in Fig. 7,*c* when step changes take place in the load torque.

Figure 8 shows the superiority of the FPI-EKF controller compared to the traditional Proportional-Integral PI-EKF either in the overshoot or in the harmonic's noises.

In other stage of studying, using VSC with SM, we have tested the strength of our controllers, with load torque applied as the following way: +10 N·m in 1.5 s, 0 N·m in 2.5 s, +10 N·m in 6 s, –10 N·m in 7 s, 0 N·m in 8 s.

The comparison in Fig. 9,*a*,*b*,*c* reveals that the observation by ELO or EKF of the electromagnetic torque.

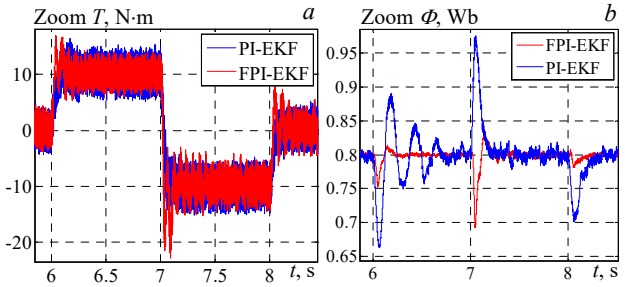

Fig. 8. Estimated electromagnetic torque *T* (*a*); «*d* axe» flux in (*b*)

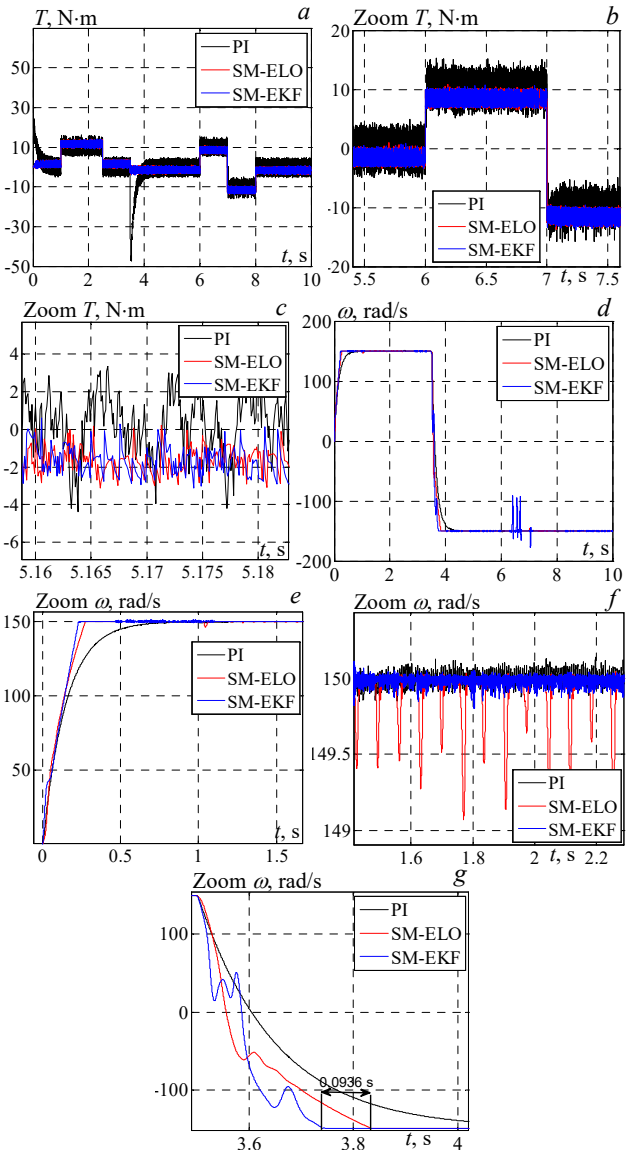

Fig. 9. Simulation results of the improved EKF and ELO observer by SM control: observed electromagnetic torque in (*a* and *b*); harmonics observed during electromagnetic control in (*c*); comparison between SM-ELO and SM-EKF speed in (*d*); comparison between SM-ELO and SM-EKF speed response time in (*e*); harmonics observed during speed control in (*f*); comparison between SM-ELO and SM-EKF speed delay time during speed reference change in (*g*)

Conclusions. The high-performance intelligent sensorless based variable structure control in an indirect rotor field oriented control scheme, of the induction motor drive, using Luenberger and extended Kalman filter observers is discussed in this literature. The robustness of the speed response using two different observers design has been compared, and it has been found to be favorable.

The results investigation confirms that the combination of sliding mode with adaptive observers achieves a pleasing performance even in the presence of noises or variations in the induction motor parameters and drive conditions. Moreover, it can be said from the results that the estimation of rotor speed has been done satisfactorily, and the sliding mode extended Kalman filter has better characteristics than the other observer presented.

Conflict of interest. The authors of the article declare that there is no conflict of interest.

REFERENCES

1. Ren Y., Wang R., Rind S.J., Zeng P., Jiang L. Speed sensorless nonlinear adaptive control of induction motor using combined speed and perturbation observer. *Control Engineering Practice*, 2022, vol. 123, art. no. 105166. doi: https://doi.org/10.1016/j.conengprac.2022.105166.

2. Chen C., Yu H., Gong F., Wu H. Induction Motor Adaptive Backstepping Control and Efficiency Optimization Based on Load Observer. *Energies*, 2020, vol. 13, no. 14, art. no. 3712. doi: https://doi.org/10.3390/en13143712.

3. Ammar A., Benakcha A., Bourek A. Adaptive MRAC-based direct torque control with SVM for sensorless induction motor using adaptive observer. *The International Journal of Advanced Manufacturing Technology*, 2017, vol. 91, no. 5-8, pp. 1631-1641. doi: https://doi.org/10.1007/s00170-016-9840-5.

4. Nguyen N.-D., Nam N.N., Yoon C., Lee Y.Il. Speed Sensorless Model Predictive Torque Control of Induction Motors Using a Modified Adaptive Full-Order Observer. IEEE *Transactions on Industrial Electronics*, 2022, vol. 69, no. 6, pp. 6162-6172. doi: https://doi.org/10.1109/TIE.2021.3094493.

5. Yin S., Huang Y., Xue Y., Meng D., Wang C., Lv Y., Diao L., Jatskevich J. Improved Full-Order Adaptive Observer for Sensorless Induction Motor Control in Railway Traction Systems Under Low-Switching Frequency. *IEEE Journal of Emerging and Selected Topics in Power Electronics*, 2019, vol. 7, no. 4, pp. 2333-2345. doi: https://doi.org/10.1109/JESTPE.2019.2898875.

6. Huang S., Deng X., Xing P., Su C. Improved Design of Feedback Matrix of Adaptive Observer for Induction Motor. *Journal of Physics: Conference Series*, 2023, vol. 2479, no. 1, art. no. 012015. doi: https://doi.org/10.1088/1742-6596/2479/1/012015.

7. Zhao H., Eldeeb H.H., Wang J., Kang J., Zhan Y., Xu G., Mohammed O.A. Parameter Identification Based Online Noninvasive Estimation of Rotor Temperature in Induction Motors. *IEEE Transactions on Industry Applications*, 2021, vol. 57, no. 1, pp. 417-426. doi: https://doi.org/10.1109/TIA.2020.3039940.

8. Pudari M., Arya S.R., Arya R.K. An improved Sliding Mode Observer for parameter estimation in induction motor drive with optimised gains. *Australian Journal of Electrical and Electronics Engineering*, 2023, vol. 20, no. 3, pp. 235-250. doi: https://doi.org/10.1080/1448837X.2023.2174110.

9. Yang Z., Zhang D., Sun X., Ye X. Adaptive Exponential Sliding Mode Control for a Bearingless Induction Motor Based on a Disturbance Observer. *IEEE Access*, 2018, vol. 6, pp. 35425-35434. doi: https://doi.org/10.1109/ACCESS.2018.2851590.

10. Zhang Y., Yin Z., Liu J., Tong X. Design and implementation of an adaptive sliding-mode observer for sensorless vector controlled induction machine drives. *Journal of Electrical Engineering and Technology*, 2018, vol. 13, no. 3, pp. 1304-1316. doi: https://doi.org/10.5370/JEET.2018.13.3.1304.

11. Ye S., Yao X. A Modified Flux Sliding-Mode Observer for the Sensorless Control of PMSMs With Online Stator Resistance and Inductance Estimation. *IEEE Transactions on Power Electronics*, 2020, vol. 35, no. 8, pp. 8652-8662. doi: https://doi.org/10.1109/TPEL.2019.2963112.

12. Mynar Z., Vaclavek P., Blaha P. Synchronous Reluctance Motor Parameter and State Estimation Using Extended Kalman Filter and Current Derivative Measurement. *IEEE Transactions on Industrial Electronics*, 2021, vol. 68, no. 3, pp. 1972-1981. doi: https://doi.org/10.1109/TIE.2020.2973897.

13. Chaabane H., Khodja D.E., Chakroune S., Hadji D. Model reference adaptive backstepping control of double star induction machine with extended Kalman sensorless control. *Electrical Engineering & Electromechanics*, 2022, no. 4, pp. 3-11. doi: https://doi.org/10.20998/2074-272X.2022.4.01.

14. Chaabane H., Eddine K.D., Salim C. Sensorless backstepping control using a Luenberger observer for double-star induction motor. *Archives of Electrical Engineering*, 2020, vol. 69, no. 1, pp. 101-116. doi: https://doi.org/10.24425/aee.2020.131761.

15. Saifi R. Implementation of a new flux rotor based on model reference adaptive system for sensorless direct torque control modified for induction motor. *Electrical Engineering & Electromechanics*, 2023, no. 2, pp. 37-42. doi: https://doi.org/10.20998/2074-272X.2023.2.06.

16. You J., Wu W., Wang Y. An Adaptive Luenberger Observer for Speed-Sensorless Estimation of Induction Machines. *2018 Annual American Control Conference (ACC)*, 2018, pp. 307-312. doi: https://doi.org/10.23919/ACC.2018.8431006.

17. Harini B.W. The Effect of Motor Parameters on the Induction Motor Speed Sensorless Control System using Luenberger Observer. *International Journal of Applied Sciences and Smart Technologies*, 2022, vol. 4, no. 1, pp. 59-74. doi: https://doi.org/10.24071/ijasst.v4i1.4518.

18. Mehdi A., Reama A., Benalla H. Two vector based direct power control of AC/DC grid connected converters using a constant switching frequency. *Journal of Power Electronics*, 2017, vol. 17, no. 5, pp. 1363-1371. doi: https://doi.org/10.6113/JPE.2017.17.5.1363.

19. Ganthia B.P., Barik S.K. Fault Analysis of PI and Fuzzy-Logic-Controlled DFIG-based Grid-Connected Wind Energy Conversion System. *Journal of The Institution of Engineers (India): Series B*, 2022, vol. 103, no. 2, pp. 415-437. doi: https://doi.org/10.1007/s40031-021-00664-9.

20. Mehedi I.M., Saad N., Magzoub M.A., Al-Saggaf U.M., Milyani A.H. Simulation Analysis and Experimental Evaluation of Improved Field-Oriented Controlled Induction Motors Incorporating Intelligent Controllers. *IEEE Access*, 2022, vol. 10, pp. 18380-18394. doi: https://doi.org/10.1109/ACCESS.2022.3150360.

21. Elgbaily M., Anayi F., Packianather M. Performance Improvement Based Torque Ripple Minimization for Direct Torque Control Drive Fed Induction Motor Using Fuzzy Logic Control. *Lecture Notes in Electrical Engineering*, 2022, vol. 921 LNEE, pp. 416-428. doi: https://doi.org/10.1007/978-981-19-3923-5_36.

22. Wogi L., Ayana T., Morawiec M., Jąderko A. A Comparative Study of Fuzzy SMC with Adaptive Fuzzy PID for Sensorless Speed Control of Six-Phase Induction Motor. *Energies*, 2022, vol. 15, no. 21, art. no. 8183. doi: https://doi.org/10.3390/en15218183.

23. Salahuddin H., Imdad K., Chaudhry M.U., Nazarenko D., Bolshev V., Yasir M. Induction Machine-Based EV Vector Control Model Using Mamdani Fuzzy Logic Controller. *Applied Sciences*, 2022, vol. 12, no. 9, art. no. 4647. doi: https://doi.org/10.3390/app12094647.

24. Benbouhenni H. Seven-level NPC Inverter-based Neuronal Direct Torque Control of the PMSM Drives with Regulation Speed Using Neural PI Controller. *International Journal of Intelligent Information Systems*, 2019, vol. 8, no. 5, pp. 85-96. doi: https://doi.org/10.11648/j.ijiis.20190805.11.

25. Chatterjee A. Analysis of a Self-Excited Induction Generator With Fuzzy PI Controller for Supporting Domestic Loads in a Microgrid. *Journal of Fuzzy Systems and Control*, 2023, vol. 1, no. 2, pp. 61-65, doi: https://doi.org/10.59247/jfsc.v1i2.42.

Received 13.08.2023
Accepted 06.11.2023
Published 02.03.2024

Khoudir Abed [1], *Doctor on Electrical Engineering, Professor,*
Hamed Kamel Eddine Zine[1], *PhD Student,*
[1] Laboratory of Electrical Engineering of Constantine (LGEC), Mentouri University, Road Ain El Bey, Constantine, Algeria,
e-mail: khoudir.abed@laposte.net (Corresponding Author);
kamel-eddine.zine-hamed@lec-umc.org

How to cite this article:
Abed K., Zine H.K.E. Intelligent fuzzy back-stepping observer design based induction motor robust nonlinear sensorless control. *Electrical Engineering & Electromechanics*, 2024, no. 2, pp. 10-15. doi: https://doi.org/10.20998/2074-272X.2024.2.02